

Polythiophene Derivatives for Efficient All-Polymer Solar Cells

Mingwei An, Qingqing Bai, Sang Young Jeong, Jianwei Ding, Chaoyue Zhao, Bin Liu, Qiming Liang, Yimei Wang, Guangye Zhang, Han Young Woo, Xiaohui Qiu, Li Niu, Xugang Guo, and Huiliang Sun*

Polymerized small molecule acceptors have recently greatly facilitated the development of all-polymer solar cells (All-PSCs) with respect to the power conversion efficiencies (PCEs). However, high-performance and low-cost polymer donors for All-PSCs are still lacking, limiting further large-scale manufacturing of All-PSCs. Herein, this work designs and synthesizes a new thiophene derivative, FETVT, featuring vinyl-bridged fluorine and ester-substituted monothiophene. Incorporation of FETVT into a polymer yields a high-performance polythiophene derivative PFETVT-T, which exhibits deep-lying HOMO level, suitable solution pre-aggregation ability, finely-tuned polymer crystallinity, and appropriate thermodynamic miscibility with the polymer acceptor L15. As a result, binary based on PFETVT-T achieves a record PCE of 11.81% with a good stability, representing a breakthrough for polythiophenes and their derivatives-based All-PSCs, which is also significantly higher than that (1.92%) of All-PSCs based on its isomerized analog. Remarkably, PFETVT-T achieves an impressive PCE exceeding 16% via the implementation of a ternary blend design. These findings offer a hopeful pathway toward attaining high-performance, stable, and cost-effective PSCs.

the development of polymerized small-molecule acceptors (PSMAs) strategy, the power conversion efficiency (PCE) of All-PSCs has now surpassed 16%.^[6–9] However, the large-scale industrial production of organic photovoltaics is hindered by the complex synthesis and high production costs of high-performance organic photovoltaic materials.^[10–12] The most efficient polymer donors are conjugated polymers comprising of alternating electron-rich and electron-deficient building blocks,^[13–15] which possess fused-ring structures making them difficult to synthesize and thus resulting in high production costs.^[16–18] Consequently, low-cost yet high-performance polymer photovoltaic materials are urgently needed to enable large-scale production of PSCs.^[19–22] Polythiophenes and their derivatives (PTs) have gained significant attention as promising candidates for large-scale

and low-cost synthesis. This is primarily attributed to their simple chemical structures and the availability of inexpensive raw materials.^[20,23–27] Intensive attentions have been devoted to improving the performance of PTs:SMAs blend systems, recently, resulting in successful PCEs of 17%.^[23] However, less attention

1. Introduction

All-polymer solar cells (All-PSCs) have drawn enormous attention in recent years due to their advantages of thermal stability and mechanical flexibility and stretchability.^[1–5] Benefitting from

M. An, Q. Bai, Q. Liang, L. Niu, H. Sun
Center for Advanced Analytical Science
Guangzhou Key Laboratory of Sensing Materials and Devices
Guangdong Engineering Technology Research Center for Photoelectric Sensing Materials and Devices
c/o School of Chemistry and Chemical Engineering
Guangzhou University
Guangzhou, Guangdong 510006, China
E-mail: Huiliang@gzhu.edu.cn

M. An, B. Liu, Y. Wang, X. Guo
Department of Materials Science and Engineering
Southern University of Science and Technology (SUSTech)
Shenzhen, Guangdong 518055, China

S. Y. Jeong, H. Y. Woo
Department of Chemistry
College of Science
Korea University
Seoul 02841, South Korea

J. Ding, X. Qiu
CAS Key Laboratory of Standardization and Measurement for Nanotechnology
CAS Center for Excellence in Nanoscience
National Center for Nanoscience and Technology
Beijing 100190, P. R. China

J. Ding, X. Qiu
University of Chinese Academy of Sciences
Beijing 100049, P. R. China
C. Zhao, G. Zhang
College of New Materials and New Energies
Shenzhen Technology University
Shenzhen 518118, China

 The ORCID identification number(s) for the author(s) of this article can be found under <https://doi.org/10.1002/aenm.202301110>

DOI: 10.1002/aenm.202301110

has been paid to PTs-based All-PSCs, leading to relatively low PCEs, generally below 8%.^[28–34] To achieve high-performance PTs-based All-PSCs, two critical challenges must be addressed. First, the mismatch of energy levels between PTs and polymer acceptors, particularly the prevailing PSMA, caused a small open-circuit voltage (V_{OC}) in All-PSCs. For instance, PTs blended with the benchmark PSMA PYT yielded an extremely poor PCE of 1.65% with a V_{OC} of 0.48 V only.^[35] Second, PTs show strong π - π stacking of polymer backbone and high crystallinity which makes it difficult to achieve the desired active layer morphology,^[36–39] thus limiting the short-circuit current density (J_{SC}) and fill factor (FF) of All-PSCs.^[25,37] Therefore, it is essential to create novel PTs that possess compatible energy levels and thermodynamically appropriate miscibility with cutting-edge PSMA to achieve All-PSCs. The development of high-performance PTs hinges on the discovery of thiophene derivatives with optimized geometry and electronic properties.^[27,40–42]

The incorporation of electron-withdrawing substituents at the β -position of thiophene represents an effective approach to reducing its electron-donating properties, resulting in deep highest occupied molecular orbital (HOMO) levels for the corresponding conjugated polymers. The successful application of halogen, ester, and cyano-substituted thiophene moieties on the main chain of polymers has been demonstrated in the development of high-performance SMA-based PSCs.^[43,44] To further enhance the synergistic effects of these functional groups, they have been simultaneously incorporated into both the main chains and side chains of polymers.^[45–47] However, increasing the thiophene content in polymers may have adverse effects on optimizing the HOMO levels, and lead to strong crystallinity, resulting in inadequate miscibility between the polymer donors and acceptors. To address this issue, our research group has previously designed and synthesized a novel thiophene derivative, FE-T, featuring a monothiophene unit functionalized with an electron-withdrawing fluorine atom (F) and an ester group (E).^[48] The resulting polymer S1 was found to have fine-tuned energy levels and crystallinity, as well as appropriate miscibility between S1 and SMA Y6.^[49] Additionally, Hou et al. reported a series of poly(thienylene vinylene) derivatives. The vinylene bridge resulted in high mobility, good solubility, and strong solution pre-aggregation for these PTs,^[20,26] showing PCEs close to those of state-of-the-art PSCs.

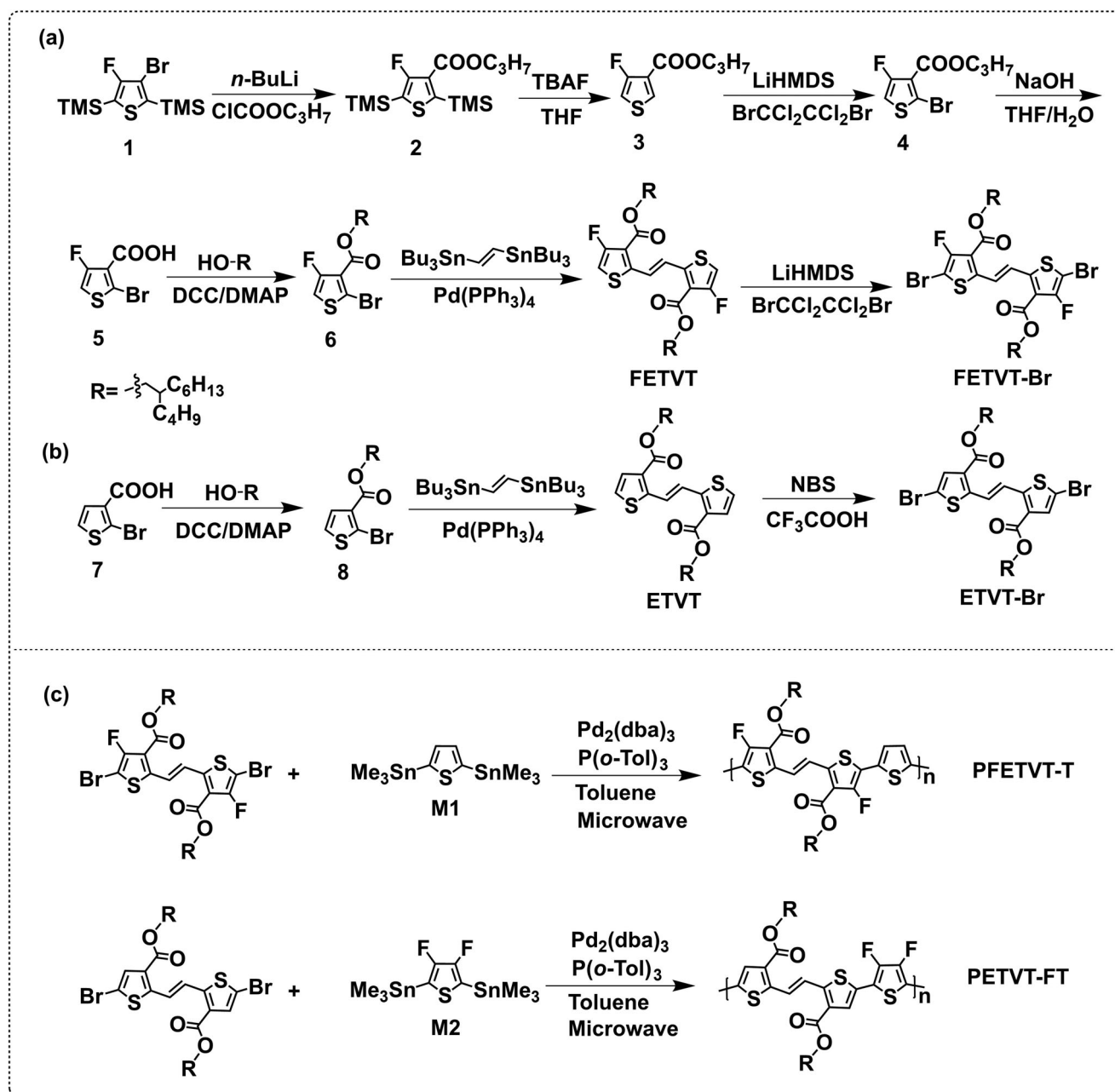
Inspired by the success of the FE-T building block and the effectiveness of vinylene bridge in improving the performance of polythiophenes-based PSCs, we have designed and synthesized a novel thiophene derivative building block, FETVT (Scheme 1), which features a vinyl-bridged F and E-substituted monothiophene. FETVT was then copolymerized with monothiophene to afford a new poly(thienylene vinylene) derivative, PFETVT-T. To demonstrate the synergistic impacts of FE-T and vinylene bridge on promoting All-PSC performance, PETVT-FT with isomerically F and E-substituted backbone (Scheme 1) was also synthesized. PFETVT-T with the optimized polymer electronic property resulted in exceptional performance in All-PSCs, achieving a PCE of up to 11.81%. This is a significant improvement compared to the PCE of 1.92% achieved by the All-PSC based on its polymer analogue, PETVT-FT. Furthermore, the incorporation of PFETVT-T into PM6:L15 system enabled fabrication of ternary All-PSCs, with an optimized device achieving a PCE of 16.2% due to the simultaneous enhancement of J_{SC} and FF in comparison to

the PM6:L15-based binary All-PSCs (PCE = 15.5%). The present study highlights the exceptional potential of FETVT as a promising building block for developing high-performance PTs for use in All-PSCs. The findings suggest that there is still room for further improvements in the photovoltaic performance of PETVT-FT-based All-PSCs.

2. Results and Discussion

PTs possess advantageous hole mobilities and wide band gaps, making them suitable for use with low band gap acceptors. However, the high HOMO levels limit their potential for achieving desirable V_{OC} in PSCs. As PTs have fewer sites for modification than polymers with complex chemical structures, their electronic and morphological properties are more difficult to tune. Two novel polythiophene-based polymers, PFETVT-T and PETVT-FT, were designed to improve the performance of PT-based All-PSCs (Scheme 1). We synthesized an unsymmetrical monofluorinated thiophene precursor compound 1 following literature procedures.^[49] Compound 1 was subsequently reacted with tert-butyllithium and electrophilic propyl carbonochloride to yield intermediate compound 2. Compound 2 was efficiently deprotected under the treatment of tetra-n-butylammonium fluoride to yield compound 3. Selective bromination of compound 3 using halogen-lithium hexamethyldisilazide (LiHMDS) and electrophilic dibromo-1,1,2,2-tetrachloroethane ($\text{BrCCl}_2\text{CCl}_2\text{Br}$) produced compound 4, which was hydrolyzed to yield compound 5. Esterification using 1,3-dicyclohexylcarbodiimide and 4-dimethylaminopyridine as the coupling agent and catalyst, respectively, led to the synthesis of compound 6. The key building block of FETVT was obtained through the Stille coupling reaction of compound 6 with (E)-1,2-bis(tributylstannyl)ethene. The dibrominated monomer, FETVT-Br was easily synthesized from FETVT using LiHMDS and $\text{BrCCl}_2\text{CCl}_2\text{Br}$. A novel PTs-based polymer, PFETVT-T, was synthesized using a Stille coupling-based polycondensation method between FETVT-Br and 2,5-bis(trimethylstannyl)thiophene. To compare its properties with PFETVT-T, an isomerized analog PETVT-FT was also synthesized. The details of synthesis and characterization of ^1H NMR, ^{13}C NMR, and HRMS are provided in Figures S1–S15, Supporting Information. The average molecular weight (M_n) of PFETVT-T and PETVT-FT were confirmed to be 62.2 and 71.9 kDa with relatively narrow polydispersity index (PDI) of 1.81 and 1.60, respectively. In order to investigate the thermal properties of PFETVT-T and PETVT-FT, differential scanning calorimetry (DSC) and thermogravimetric analysis (TGA) measurements were conducted (Figure S16, Supporting Information). There were no significant thermal transitions observed in the temperature range of 30 to 280 °C for both PFETVT-T and PETVT-FT, implying good thermal stability and stable amorphous for device fabrication.

To further understand of the molecular frontier orbitals and geometries of simplified trimers, density functional theory (DFT) theoretical calculations were conducted at the B3LYP/6-31G (d, p) level. These calculations aimed to provide more comprehensive fundamental properties of the studied molecules.^[50,51] Figure S19, Supporting Information, demonstrates that the PETVT-FT and PFETVT-T polymers exhibit HOMO/LUMO energy levels of $-4.99/-2.73$ eV and $-4.91/-2.76$ eV, respectively. Moreover, the π -electron orbitals are evenly distributed across the polymer



Scheme 1. Synthetic route to a) F and E-substituted thienylene vinylene monomer FETVT-Br, b) ester substituted monomer ETVT-Br and c) the corresponding isomeric polymer semiconductors PFETVT-T and PETVT-FT.

backbones. The incorporation of FE-T units caused a slight reduction in the band gap by shifting the LUMO levels down and the HOMO levels up. To investigate the energy levels of the two polymers, electrochemical cyclic voltammetry (CV) was employed, and the corresponding energy level diagrams are depicted in **Figure 1c**. The HOMO/LUMO energy levels of PETVT-FT and PFETVT-T were found to be $-5.70/-3.09$ eV and $-5.63/-3.18$ eV, respectively, which are consistent with the theoretical calculations. **Figure 1b** displays that PETVT-FT exhibits a nearly planar polymer backbone with dihedral angles close to 0° . Conversely, PFETVT-T exhibits increased dihedral angles (14.28°)

between the thiophene and ethylene groups due to the incorporation of FE-T. UV-vis absorption spectra of PETVT-FT and PFETVT-T in solution and film state were characterized as shown in **Figure 1d**. The polymer PETVT-FT displays a stronger shoulder peak absorption and obvious intensity ratio of 0.0/0.1 peaks in both solution and film state than PFETVT-T, indicating that the PETVT-FT conjugated backbone has a stronger aggregation than that of PFETVT-T.^[52–54] To investigate the aggregation behavior of PETVT-FT and PFETVT-T, we measured their temperature-dependent absorption spectra in chlorobenzene with the temperature from 30 to 90°C , as depicted in **Figure 1e,f**. The absorption

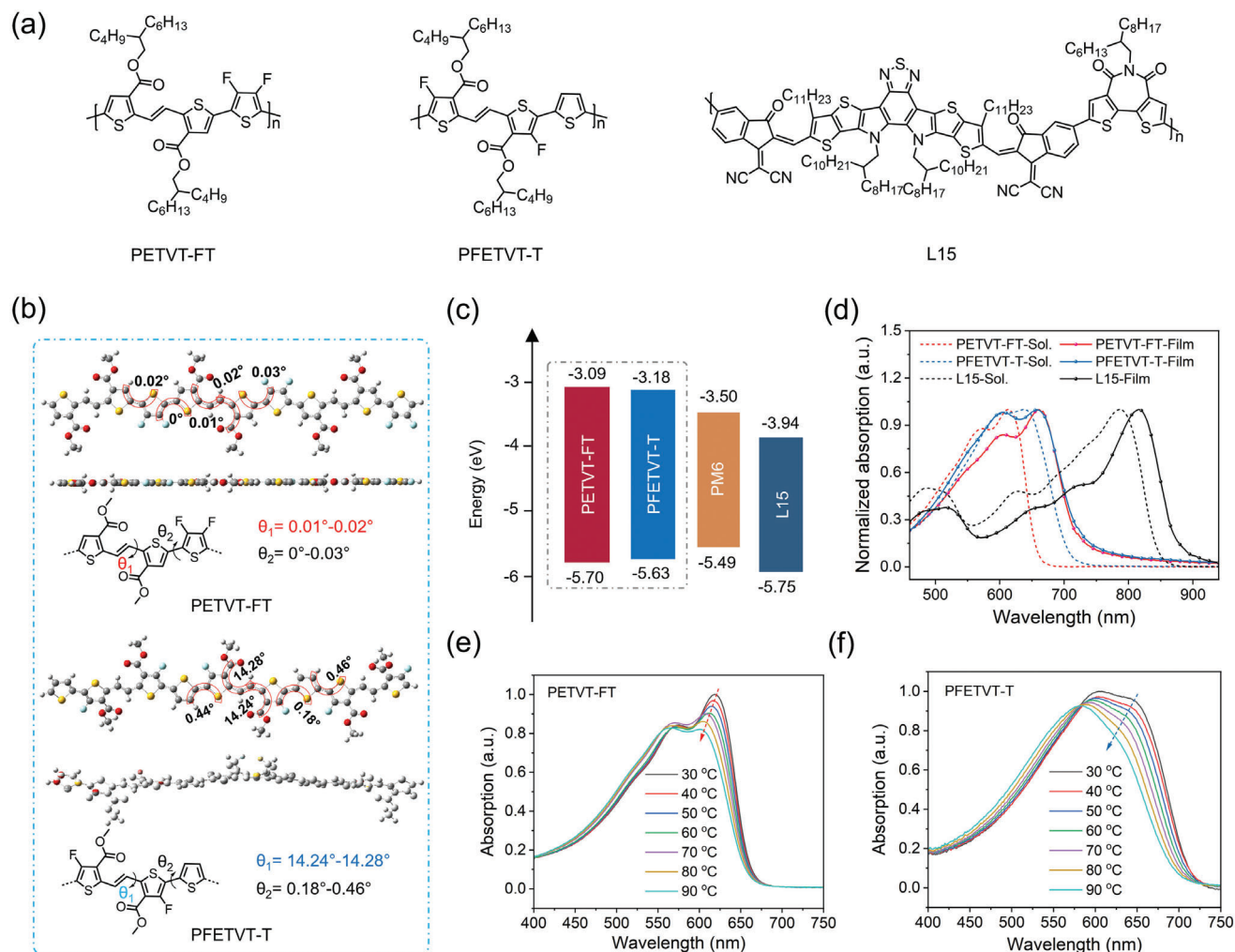


Figure 1. a) Molecule structures of PETVT-FT, PFETVT-T and L15. b) Chemical geometry models for PETVT-FT and PFETVT-T. c) Energy level diagrams of the polymers. d) UV-vis absorption spectra of PETVT-FT, PFETVT-T and L15 in solution and film state. Temperature dependent UV-vis absorption spectra of e) PETVT-FT and f) PFETVT-T in chlorobenzene.

peaks of both polymers exhibited a blue shift and decreased in intensity. Notably, at 90 °C, the 0-0 absorption peak of PETVT-FT remained, whereas that of PFETVT-T disappeared, indicating that PETVT-FT exhibits a strong pre-aggregation and a weak temperature dependence, whereas PFETVT-T displays relatively weak pre-aggregation in solution. Moreover, the 0-0 absorption peak of PFETVT-T clearly shifted from 648 to 625 nm as the temperature increased from 30 to 90 °C, while only a 15 nm blueshift was observed for PETVT-FT. This observation suggests that the aggregation of PFETVT-T is weaker than that of PETVT-FT and can be more easily disaggregated.^[55] These results are consistent with the theoretical calculation that PFETVT-T has a highly twisted backbone, which leads to a weak aggregation effect, whereas the backbone of PETVT-FT is planar, benefiting for better π - π stacking, but may hinder blending with polymer acceptors.^[56,57] The introduction of FE-T unit helps strike a delicate balance between suppressing aggregation and retaining effective intermolecular π - π interactions. This suitable aggregation property of PFETVT-T can facilitate the formation of a favorable film morphology with

polymer acceptors and thus enhance the efficiency of organic photovoltaic devices.^[58]

In order to assess the photovoltaic performance of PETVT-FT and PFETVT-T, All-PSCs devices were fabricated. A normal-type device configuration of ITO/PEDOT:PSS/polymer donor:L15/PNDIT-F3N/Ag was used in this work.^[59,60] The polymer L15 was employed as an acceptor due to its suitable electronic energy levels and complement absorption with the donors of PETVT-FT and PFETVT-T (Figure 1c,d).^[61,62] All-PSCs based on PETVT-FT:L15 and PFETVT-T:L15 were fabricated by adopting a chloroform solvent with a concentration of 18 mg mL⁻¹ and a D:A ratio of 1:1 (Table S1, Supporting Information), where D and A refer to the polymer donor and acceptor, respectively. **Figure 2a** presents the current density versus voltage (J - V) plots of the PETVT-FT:L15 and PFETVT-T:L15-based devices on the optimality conditions, and the corresponding photovoltaic data are summarized in **Table 1**. The PETVT-FT:L15-based All-PSCs achieved a PCE of 1.92% with a V_{OC} of 0.98 V, a J_{SC} of 3.76 mA cm⁻² and an FF of 52.43%.

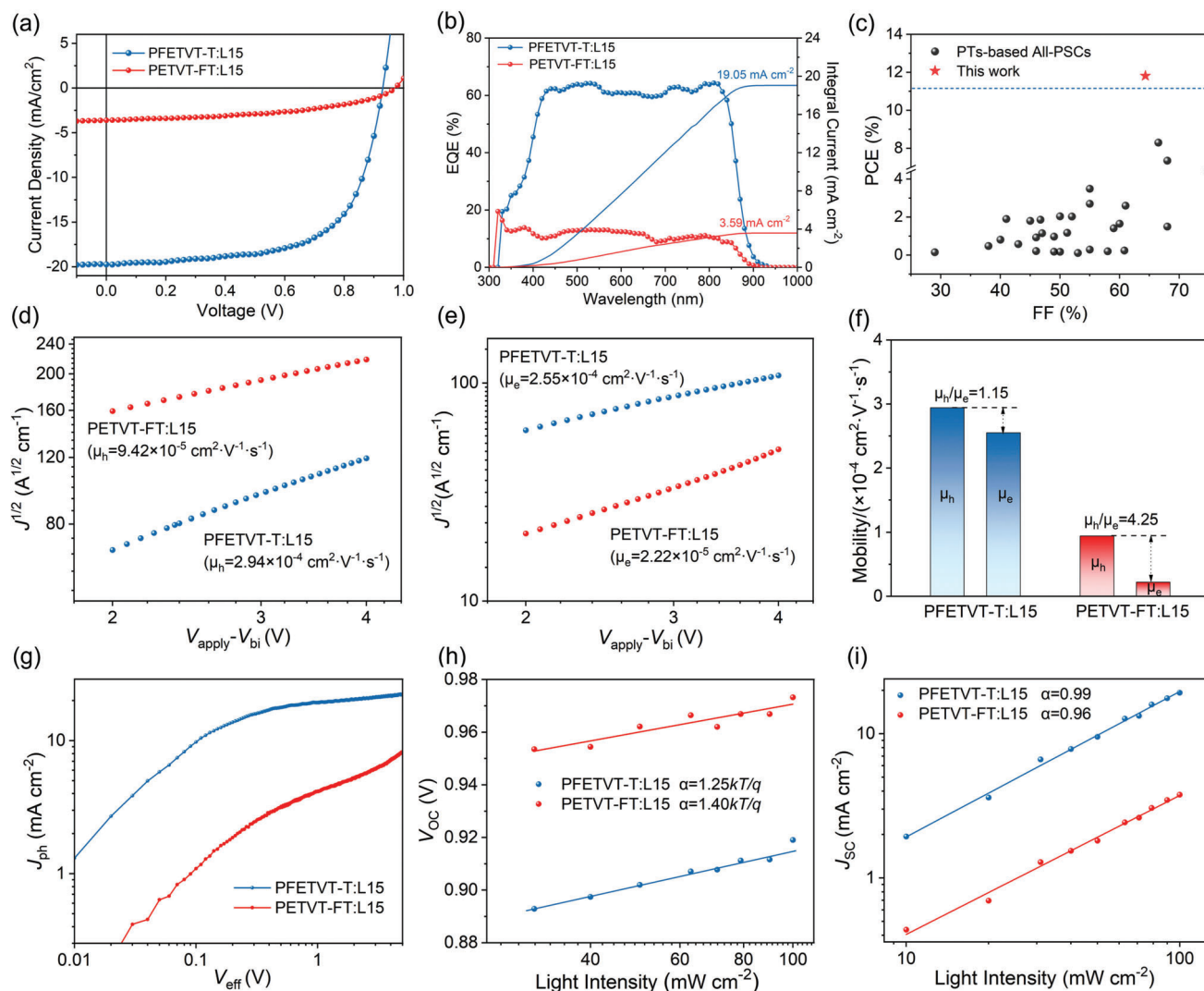


Figure 2. a) J - V and b) EQE curves of All-PSCs devices based on PFETVT-T:L15 and PETVT-FT:L15, respectively. c) Plots of the PCE versus FF for the PTs-based All-PSCs with EQEs reported in the literature. d) Hole-only and e) electron-only mobilities of blends measured using SCLC approach. f) The hole/electron mobility ratios for the corresponding devices. g) J_{ph} - V_{eff} curves of PFETVT-T:L15 and PETVT-FT:L15-based All-PSCs devices. h) V_{oc} and i) J_{sc} dependence on P_{light} of two All-PSCs devices.

While the PFETVT-T:L15-based All-PSCs yielded a maximum PCE of 11.81% with a V_{oc} of 0.93 V, a J_{sc} of 19.74 mA cm^{-2} and an FF of 64.33%. As far as we know, the PCE of 11.81% achieved in this study is the highest reported to date for binary All-PSCs based on PTs (Figure 2c and Table S5, Supporting Information). Figure 2b displays the external quantum efficiency (EQE) spectra of the All-PSCs. PFETVT-T:L15-based device delivers significantly higher EQE response over 60%

than that of PETVT-FT:L15-based device (below 20%) between 300 and 900 nm, which was in line with absorption coefficient of the blend films (Figure S18, Supporting Information), implying that the PFETVT-T:L15-based All-PSCs efficiently contribute to charge generation and photon harvesting. Consequently, the PFETVT-T:L15-based All-PSCs has a higher J_{sc} of 19.04 mA cm^{-2} from EQE curves than that of PETVT-FT:L15-based (3.59 mA cm^{-2}), which is in accordance with the

Table 1. Photovoltaic performance data of the All-PSCs based on PETVT-FT:L15 and PFETVT-T:L15.

Active Layer ^{a)}	V_{oc} [V]	J_{sc} [mA cm^{-2}] ^{b)}	FF [%]	PCE [%] ^{c)}
PETVT-FT:L15	0.98 (0.97 ± 0.01)	3.76 (3.59) (3.74 ± 0.06)	52.43 (51.93 ± 1.67)	1.92 (1.89 ± 0.05)
PFETVT-T:L15	0.93 (0.92 ± 0.01)	19.74 (19.04) (19.64 ± 0.15)	64.33 (64.23 ± 0.48)	11.81 (11.69 ± 0.12)

^{a)} The device area is 3.7 mm^2 ; ^{b)} The integrated J_{sc} values from the EQE spectra; ^{c)} The average PCEs in brackets were calculated from 15 devices.

results measured from J - V curves. To evaluate the chemical complexity and experimental effort required in the synthesis, we analyzed the synthetic complexity (SC) to quantify the effect of our strategy on figure of merit (FOM).^[63] As shown in Table S13, Supporting Information, PFETVT-T and PETVT-FT have a decent SC value compared with the prevailing polymer donors, and lower than that of the benchmark polymer donor PM6. While the FOM value of PFETVT-T is 0.22 higher than that of PETVT-FT (0.05), indicative of the stronger potential for application. The ternary All-PSCs demonstrated more balanced charge mobility and less energy loss than the corresponding binary device.^[64,65] The polymers of PFETVT-T, PM6 and L15 present stepwise energy level alignments (Figure 1c) and complementary absorption bands, suggesting that they may develop an efficient ternary All-PSCs. We optimized the PFETVT-T/PM6/L15 weight ratio and 1-chloronaphthalene (CN) content for PFETVT-T:PM6:L15-based devices (Tables S11 and S12, Supporting Information). The ternary device with the best weight ratio of 0.05:0.95:1 and containing 2% (v/v) CN as the additive shows a PCE of 16.15% ($V_{OC} = 0.92$ V, $J_{SC} = 24.72$ mA cm⁻², FF = 71.23%). Compared with PM6:L15 devices, the ternary-blend devices gave a higher J_{SC} , which should benefit from their complementary light absorption.

The charge mobilities of the polymer neat films and blend films were measured using the space-charge limited current (SCLC) method, as depicted in Figure 2d,e and Figure S21, Supporting Information.^[59,66] The polymer PFETVT-T exhibited a higher μ_h of 1.82×10^{-4} cm² V⁻¹ s⁻¹ than that of the PETVT-FT counterpart ($\mu_h = 9.69 \times 10^{-6}$ cm² V⁻¹ s⁻¹), which facilitates charge extraction. The average μ_h/μ_e s of PETVT-FT:L15 and PFETVT-T:L15 devices are $9.42 \times 10^{-5}/2.22 \times 10^{-5}$ and $2.94 \times 10^{-4}/2.55 \times 10^{-4}$ cm² V⁻¹ s⁻¹, respectively. Notably, the charge transport of PFETVT-T:L15 blend with a μ_h/μ_e ratio of 1.15 was more balanced than that of (4.25) in PETVT-FT:L15 blend (Figure 2f). This result demonstrates that the position of F and E-substituted PTs backbone influences the carrier transport properties of the blend. Compared with PETVT-FT, the enhanced and well-balanced charge transport in the PFETVT-T-based blend films contributes to impeding charge accumulation and recombination, resulting in higher FF to the corresponding devices.^[67] To explore the synergistic effect of FE-T and vinylene bridge on the exciton generating and dissociation, the dependence of photocurrent density (J_{ph}) versus effective voltage (V_{eff}) for the PETVT-FT:L15 and PFETVT-T:L15 devices was examined and is shown in Figure 2g. In the equation $J_{ph} = J_L - J_D$, J_{ph} represents the photocurrent density, which is the difference between the current densities under illumination J_L and in the dark J_D . The V_{eff} is determined by subtracting the V_{bis} from the applied V_0 at which the photocurrent density is zero.^[68,69] The exciton dissociation and charge collection probability (P_c) of the two devices can be characterized by the J_{ph}/J_{sat} values, where J_{sat} is the saturation current density. As shown in Table S7, Supporting Information, the P_c s of PETVT-FT:L15 and PFETVT-T:L15-based devices are measured to be 44.46% and 83.46%. The higher P_c value of PFETVT-T:L15-based device than PETVT-FT:L15-based device indicates that the superior photovoltaic performance of the PFETVT-T:L15-based device can be attributed to more efficient exciton generation and charge collection, compared to the PETVT-FT:L15-based device.^[70,71]

To further study why the PFETVT-T:L15-based devices can gain both higher J_{SC} and FF values compared with PETVT-FT:L15-based devices, their charge recombination mechanism were investigated. The slope of V_{OC} relative to light intensity (P_{light}) is equal to kT/q (Figure 2h).^[72,73] The PFETVT-T:L15-based device gives a slope value of 1.25 kT/q, while for PETVT-FT:L15-based device, the slope is 1.40 kT/q, indicating that trap-assisted recombination is efficiently mitigated in the PFETVT-T:L15-based device.^[39] The relationship between J_{SC} and P_{light} can be expressed as $J_{SC} \propto P_{light}^\alpha$, as shown in Figure 2i. The α values in PFETVT-T:L15 and PETVT-FT:L15-based devices are 0.99 and 0.96, indicating that PFETVT-T:L15-based All-PSCs has negligible bimolecular recombination because its α value is closer to 1.^[74] Furthermore, the photoluminescence (PL) spectra of neat polymer and the blends were carried out to evaluate the charge dissociation characteristics at D:A interfaces. As shown in Figure S23, Supporting Information, after blending with L15, the quenching efficiency of PFETVT-T:L15 blend is 84.28% higher than that of PETVT-FT:L15 blend (31.20%). The better PL quenching efficiency of PFETVT-T:L15 demonstrates that more effective exciton dissociation takes place in the PFETVT-T:L15 interfaces, which is attributed to the more mixing of PFETVT-T and L15 in blend.

Transient absorption (TA) spectroscopy measurements further were employed to gain more insights into the charge transfer process and recombination dynamics of the two All-PSCs.^[75,76] Figure S24, Supporting Information displays the TA spectra of PETVT-FT, PFETVT-T and L15 neat films. The ground state bleaching (GSB) signal of the PETVT-FT neat film was observed in the range of 550–660 nm, while PFETVT-T shows red-shifted GSB peaks in 580–700 nm. For the L15 neat film, a broad GSB signal mainly located at 630–750 nm can be observed. To study the details of hole transfer process from the acceptor to the donor in blends, a pumping wavelength of 800 nm was chosen to selectively excite L15. As shown in Figure 3a–d, the GSB signals of the PETVT-FT:L15 and PFETVT-T:L15 blends exhibit a delayed rising centered at ≈ 630 and 650 nm, respectively, matching very well with the GSB signals of the corresponding donor, implying interfacial hole transfer from L15 to both PETVT-FT and PFETVT-T. To further assess the hole transfer dynamics of the PETVT-FT:L15 and PFETVT-T:L15 blends, we extracted the kinetic profiles of GSB signals at 638 and 673 nm for PETVT-FT and PFETVT-T in the blend films. As shown in Figure S25, Supporting Information, the GSB signal of donor is superimposed on the kinetics of charge transfer signals in both blends, but it's clear that charge transfer signal of PFETVT-T:L15 film shows a faster rise than that of PETVT-FT:L15 film, suggesting that the PFETVT-T possesses a faster interfacial hole transfer rate. The faster hole transfer process in PFETVT-T:L15 blend film is beneficial for the photogenerated charge carrier extraction and collection, which agrees well with the higher FF and more efficient EQE response. We further study the recombination mechanism by varying the pump power. As shown in Figure S26, Supporting Information, the kinetics show a negligible power-dependence from 2 to 15 μ W, indicating that geminate recombination is the dominant mechanism in the PETVT-FT:L15 and PFETVT-T:L15 blends.^[77]

To explore the energy loss in two devices, a comprehensive analysis of E_{loss} was conducted by tests and calculations such as

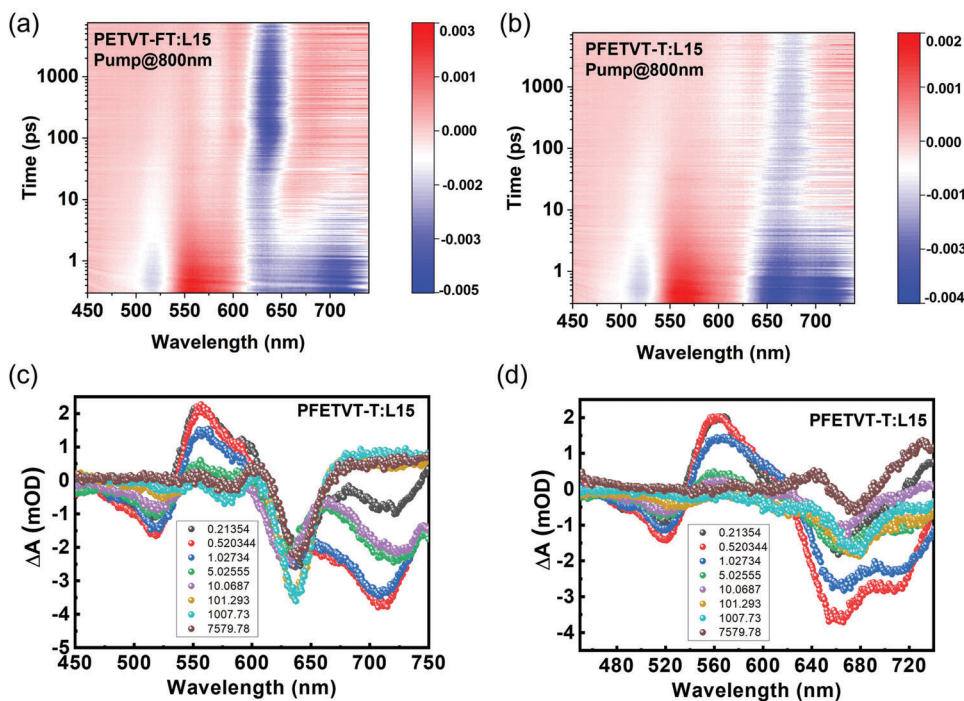


Figure 3. 2D TA images of the a) PETVT-FT:L15 and b) PFETVT-T:L15 blend films. TA spectra of c) PETVT-FT:L15 and d) PFETVT-T:L15 blend films at different time delays.

fourier transform photocurrent spectroscopy (FTPS) and electroluminescence (EL) spectroscopy, as depicted in Figure S22, and Table S8, Supporting Information. According to the principles of detailed balance theory, the overall E_{loss} in organic solar cells comprises both radiative recombination loss and nonradiative recombination loss. The optical bandgap (E_{gap}) was determined by analyzing the points of intersection between the normalized absorption and EL spectra of the films. The energy loss can be divided into three main factors, which are defined in Equation (1). The detailed E_{loss} parameters for PETVT-FT:L15 and PFETVT-T:L15-based devices are summarized in Table S8, Supporting Information.

$$\begin{aligned} E_{\text{loss}} &= E_{\text{gap}} - V_{\text{OC}} \\ &= (E_{\text{gap}} - qV_{\text{OC}}^{\text{SQ}}) + (qV_{\text{OC}}^{\text{SQ}} - qV_{\text{OC}}^{\text{rad}}) + (qV_{\text{OC}}^{\text{rad}} - qV_{\text{OC}}) \\ &= \Delta E_1 + \Delta E_2 + \Delta E_3 \end{aligned} \quad (1)$$

ΔE_1 represents the intrinsic radiative energy loss occurring above the bandgap. The calculated values of ΔE_1 for PETVT-FT:L15 and PFETVT-T:L15-based devices were determined to be 0.265 and 0.264 eV, respectively. The charge transfer state energy (E_{CT}) of the two All-PSCs were calculated by fitting FTPS-EQE and EL spectra (Figure S22, Supporting Information). Compared with PFETVT-T:L15-based devices ($E_{\text{CT}} = 1.40$ eV), PETVT-FT:L15-based devices present a slightly higher E_{CT} value of 1.42 eV. The ΔE_2 was estimated to be 0.278 eV for PETVT-FT:L15-based devices, higher than that of PFETVT-T:L15-based devices (0.176 eV). $E_{\text{g}} - E_{\text{CT}}$ is recognized as a key driving force for charge dissociation. Research has demonstrated a strong inverse correlation between the electroluminescence external quantum efficiency (EQE_{EL}) and the driving force value, signifying that

lower driving force values are concomitant with higher EQE_{EL} . By measuring the values of EQE_{EL} , ΔE_3 ($\Delta E_3 = qV_{\text{OC}}^{\text{rad}} - qV_{\text{OC}} = q\Delta V_{\text{OC}}^{\text{non-rad}} = -kT \ln(\text{EQE}_{\text{EL}})$) was determined, which arises from non-radiative recombination processes, where k corresponds to the Boltzmann constant, T represents the absolute temperature. The ΔE_3 generated by devices based on PFETVT-T:L15 was significantly smaller than that of devices based on PETVT-FT:L15. As a result, PETVT-FT:L15-based devices showed higher E_{loss} values of 0.803 eV compared to that of PFETVT-T:L15-based devices (0.647 eV).

Grazing incidence wide-angle X-ray scattering (GIWAXS) is a powerful technique used to study the molecular packing and ordering properties of thin films. In this study, GIWAXS was used to investigate the pure films of PETVT-FT, PFETVT-T, and L15, as well as their blend films. The 2D-GIWAXS patterns and 1D line-cut profiles in the in-plane (IP) and out-of-plane (OOP) directions were analyzed. The obtained results reveal that the neat films of polymer donors, PETVT-FT and PFETVT-T, exhibit the prominent (010) π - π diffraction peaks at $\approx 1.73 \text{ \AA}^{-1}$ in the OOP directions and (100) lamellar peaks at $\approx 0.29 \text{ \AA}^{-1}$ in the IP directions, manifesting a preferential orientation relative to the substrate. As depicted in Figure 4 and Table S9, Supporting Information, the crystal coherence lengths (CCLs) of (010) in the OOP directions and (100) in the IP directions were estimated using the Scherrer equation. In comparison to the neat PETVT-FT films, which exhibit (010) π - π stacking CCLs of 34.9 Å, PFETVT-T demonstrates higher (010) π - π stacking CCLs of 40.9 Å, which is advantageous for charge transport in the vertical direction. Specifically, the estimated CCLs of (100) diffraction in the IP directions are $\approx 91.2 \text{ \AA}$ for PETVT-FT and 108.8 Å for PFETVT-T. These results indicate that the neat PFETVT-T donor films exhibit

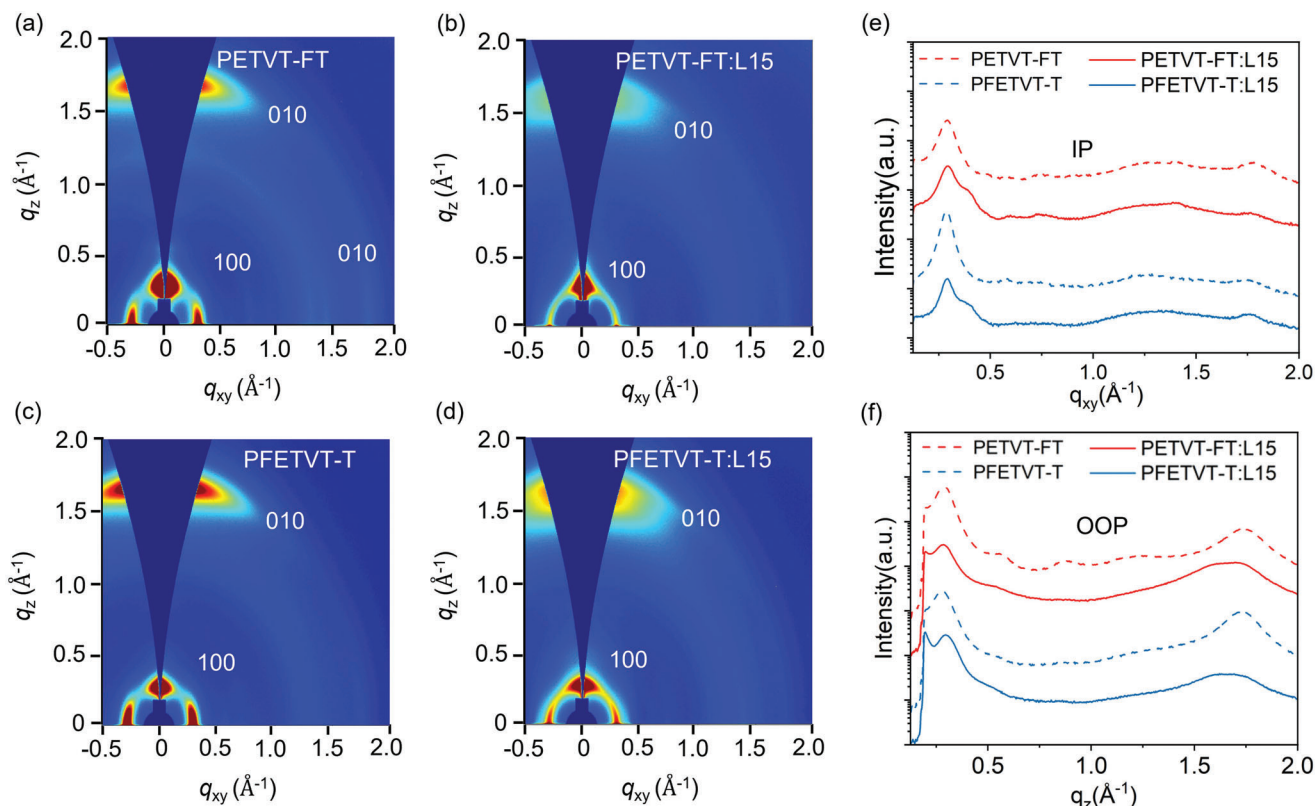


Figure 4. 2D GIWAXS patterns of a) pure PETVT-FT film, b) PETVT-FT:L15 blend film, c) pure PFETVT-T film, and d) PFETVT-T:L15 blend film. e) IP and f) OOP profiles for the corresponding films.

superior lamellar ordering compared to that of PETVT-FT, consistent with the significantly higher hole mobilities of the neat PFETVT-T donor films ($\mu_h = 1.82 \times 10^{-4} \text{ cm}^2 \text{ V}^{-1} \text{ s}^{-1}$). These findings indicate that the incorporation of the FE-T unit into PFETVT-T improves its crystalline structure, leading to enhanced ordering and alignment of molecules. After blending with L15, both blend films exhibited the predominant face-on orientation with (010) π - π diffraction peaks in the OOP directions and (100) diffraction peaks in the IP directions.^[78,79] Noteworthy, the OOP (010) diffraction peaks of the polymer donors in Figure 4c,d overlapped with polymer acceptor L15. In addition, we have performed Gaussian peak fitting to the (010) peak of the π - π stacking. As a result, both blend films could be fitted into diffraction peaks attributed to the crystallization of PFETVT-T ($q_z = 1.741 \text{ Å}^{-1}$) and L15 ($q_z = 1.620 \text{ Å}^{-1}$) or PETVT-FT ($q_z = 1.726 \text{ Å}^{-1}$) and L15 ($q_z = 1.591 \text{ Å}^{-1}$), thereby the broad (010) peaks in OOP direction for both blend films could be ascribed to the overlapped diffractions, as illustrated in Figure S27 and Table S9, Supporting Information. However, the distinct (100) lamellar peaks at $\approx 0.29 \text{ Å}^{-1}$ in the IP directions originating from the polymer donors' (100) diffraction are still discernible (Figure S27, Supporting Information), thereby facilitating efficient hole transport and resulting in high charge carrier mobility.^[54,80] These results are consistent with the SCLC mobility measurement and contributed to the efficient performance of the PFETVT-T:L15-based All-PSCs. In summary, GIWAXS analysis provided valuable insights into the molecular packing and ordering properties of the pure PT films and their blend films, which helped to understand the mecha-

nism behind the superior photovoltaic performance of PFETVT-T:L15-based All-PSCs.^[81–83]

Additionally, the polar-functional group and their position isomeric should have large impacts on the surface energy (γ) and correlate with the miscibility and phase separation of the D and A blend films. The surface energy values of the polymer neat films were examined through characterizing contact angles of water and glycerol (Figure S28, Supporting Information). The γ values are 20.79, 21.95, and 24.02 mN m⁻¹ for PETVT-FT, PFETVT-T and L15, respectively (Table S10, Supporting Information). Flory–Huggins interaction parameters (χ_{DA}) were estimated from the following empirical equation: $\chi_{DA} = \kappa(\sqrt{\gamma_D} - \sqrt{\gamma_A})^2$,^[84,85] where κ is a positive constant.^[54] A low χ_{DA} value indicated the hypermiscibility between the two components. Accordingly, PFETVT-T:L15 system acquired a smaller χ_{DA} value of 0.04κ than that of PETVT-FT:L15 system (0.12κ), suggesting the much-improved miscibility of the PFETVT-T:L15 blend film, leading to a well-formed morphology. To investigate the morphology of the blend films under optimal device conditions, atomic force microscopy (AFM) and transmission electron microscopy (TEM) were employed and the results are presented in Figure 5. The AFM height images revealed that the PFETVT-T:L15 blend film exhibited a smaller root-mean-square (RMS) roughness of 0.97 nm, which is significantly lower compared to the PETVT-FT:L15 blend film's 1.42 nm, indicating a smoother surface and more evenly distributed nanofiber structures. This finding suggested that the PFETVT-T:L15 active layer had better miscibility, leading to improved device performance.^[86,87] Furthermore, TEM

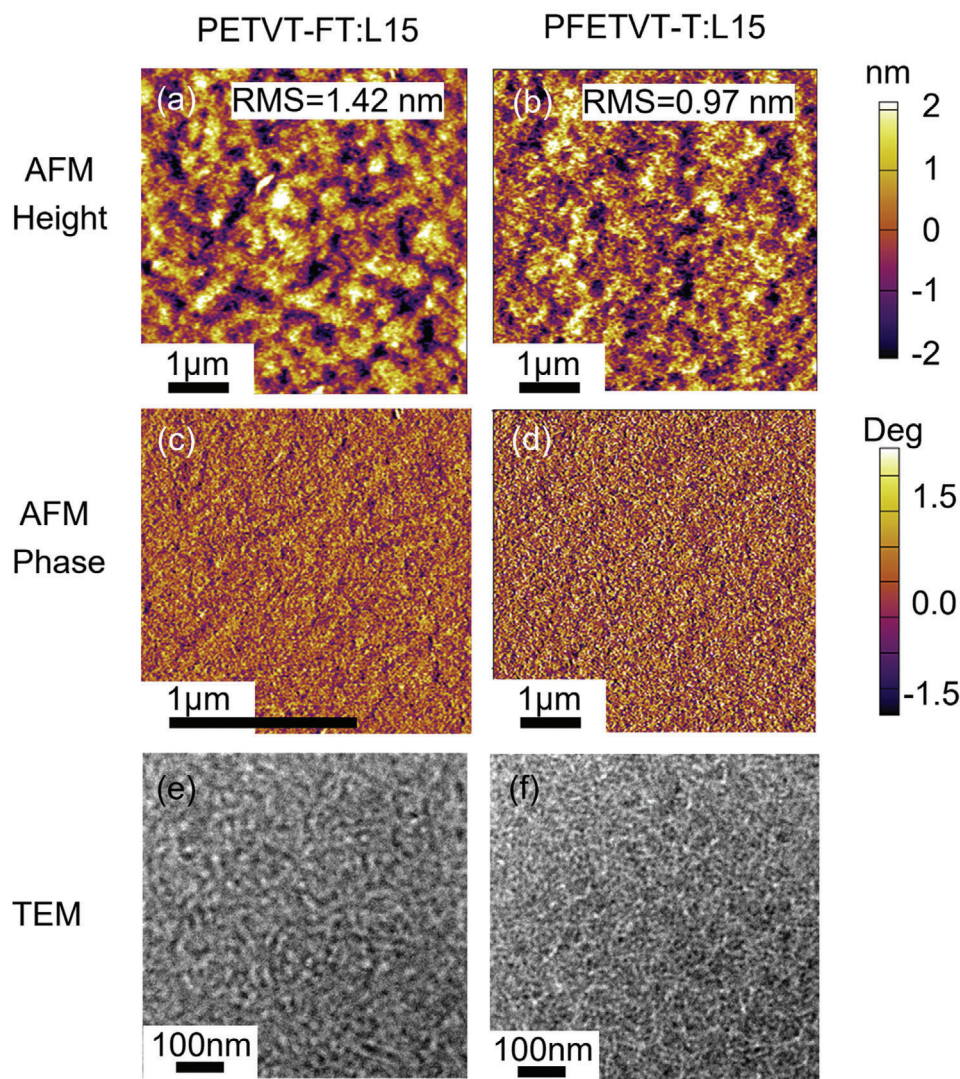


Figure 5. a,b) AFM height images, c,d) phased images, e,f) TEM images of PETVT-FT:L15 and PFETVT-T:L15 blend films.

micrographs displayed noticeable differences between the PETVT-FT:L15 and PFETVT-T:L15 blend films. As demonstrated in Figure 5e,f, the PFETVT-T:L15 blends exhibited homogeneous nanoscale phase separation micro-morphology. These results indicated that introducing of FE-T and vinylene bridge into PTs can effectively enhance molecule ordering and nanoscale phase separation, thereby contributing to higher carrier mobility and J_{SC} .

To evaluate the stability of two systems, the stabilized photocurrent and PCEs of the devices based at the maximum power point ($MPP_{PETVT-FT:L15} = 0.68$ V and $MPP_{PFETVT-T:L15} = 0.73$ V) were measured. As depicted in Figure S29, Supporting Information, the stabilized power output (SPO) for PETVT-FT:L15 and PFETVT-T:L15 processed devices remained at 1.56% and 11.96%, respectively, after a duration of 350 s, indicating that the PFETVT-T:L15-based all-PSCs keep good stability under MPP tracking. In addition, the $J-V$ characteristics of the All-PSCs based on PETVT-FT:L15 and PFETVT-T:L15 were tracked and tested under illumination, darkness and thermal aging conditions for more than 500 h, respectively (Figure S30, Supporting Information).^[88,89] After

being exposed to white LED light with an intensity of 100 mW cm^{-2} for 500 h, the PFETVT-T:L15-based device experienced a decline in performance to 90%. Following a storage period of 500 h at room temperature, PFETVT-T:L15-based All-polymer devices experienced a slight decrease in efficiency but still retained $\approx 90\%$ of its original efficiency. Furthermore, subjecting the PETVT-FT:L15-based device to continuous thermal stress at 60°C for 150 h resulted in a significant reduction of efficiency, with only 60% of the initial PCE remaining. In contrast, the PFETVT-T:L15-based devices exhibited remarkable thermal stability, retaining 80% of its original PCE after 500 h of thermal aging. These results indicate that the high miscibility of the PFETVT-T:L15 blend film exhibits better morphological stability.

3. Conclusion

In this study, we have introduced a novel thiophene derivative building block, FETVT, which features a vinyl-bridged fluorine and ester-substituted monothiophene. This unique

molecular structure enables the FETVT-based polymer with a lower-lying HOMO level and a flexible molecular backbone compared to its analog PETVT-FT, which has an isomerically fluorine and ester-substituted polymer backbone. Molecular isomerization shows significant impacts on their molecular orientation, aggregation behavior, and film morphology. It was demonstrated that PFETVT-T-based blend films exhibit a preference of face-on orientation and homogeneous nanoscale phase separation morphology, whereas PETVT-FT:L15 tends to have a bimodal molecular orientation. Thanks to its optimized geometry and electronic properties, PFETVT-T exhibits excellent All-PSC performance with a PCE of up to 11.81%, which is substantially higher than that (1.92%) achieved by the PETVT-FT-based All-PSCs. Moreover, we have successfully incorporated PFETVT-T into the PM6:L15 system to fabricate ternary All-PSCs, which achieved an even higher PCE of 16.2%. Overall, these results demonstrate that FETVT is a remarkable building block for the development of new high-performance PT-based polymer donors for All-PSCs. The unique properties of this building block provide remarkable opportunities for further optimization and improvement of the PT-based materials for a wide range of optoelectronic applications.

Supporting Information

Supporting Information is available from the Wiley Online Library or from the author.

Acknowledgements

M.A. and Q.B. contributed equally to this work. H.S. thanks the support from the National Natural Science Foundation of China (52173172), the Natural Science Foundation for Distinguished Young Scholars of Guangdong Province (2021B1515020027), the Shenzhen Science and Technology Innovation Commission (JCY202103243104813035), the Open Fund of the State Key Laboratory of Luminescent Materials and Devices (South China University of Technology, 2022-skllmd-17), the Research & Development Projects in Key Areas of Guangdong Province, China (2019B010933001), Science and Technology Projects in Guangzhou (202201000002) and Department of Science & Technology of Guangdong Province (2022A156). This work is also supported by the National Natural Science Foundation of China (52203228 and 52203227), China Postdoctoral Science Foundation (2021M700062 and 2022M711464), the Natural Science Foundation of Guangdong Province of China (2023A1515011916), Shenzhen Science and Technology Innovation Commission (JCY20180504165709042). H.Y.W. thanks the support from the National Research Foundation (NRF) of Korea (2020M3H4A3081814 and 2021M3H4A3A02086779). The authors thank Yufei Wang, Zizhou Wang, and Wei-quan Lin at the Analytical and Testing Center of Guangzhou University for the NMR and MS testing, respectively. The authors thank Dr. Yinhua Yang, Hua Li and Lin Lin at the Materials Characterization and Preparation Center SUSTech for the high temperature ^1H NMR and HRMS testing, respectively. This work was also supported by the Center for Computational Science and Engineering of SUSTech.

Conflict of Interest

The authors declare no conflict of interest.

Data Availability Statement

The data that support the findings of this study are available in the supplementary material of this article.

Keywords

all-polymer solar cells, isomerization, miscibility, morphology, polythiophenes

Received: April 13, 2023

Revised: May 28, 2023

Published online:

- [1] C. Lee, S. Lee, G.-U. Kim, W. Lee, B. J. Kim, *Chem. Rev.* **2019**, 119, 8028.
- [2] T. Kim, J.-H. Kim, T. E. Kang, C. Lee, H. Kang, M. Shin, C. Wang, B. Ma, U. Jeong, T.-S. Kim, B. J. Kim, *Nat. Commun.* **2015**, 6, 8547.
- [3] G. Wang, F. S. Melkonyan, A. Facchetti, T. J. Marks, *Angew. Chem., Int. Ed.* **2019**, 58, 4129.
- [4] L. Ma, Y. Cui, J. Zhang, K. Xian, Z. Chen, K. Zhou, T. Zhang, W. Wang, H. Yao, S. Zhang, X. Hao, L. Ye, J. Hou, *Adv. Mater.* **2023**, 35, 2208926.
- [5] G. Sun, X. Jiang, X. Li, L. Meng, J. Zhang, S. Qin, X. Kong, J. Li, J. Xin, W. Ma, Y. Li, *Nat. Commun.* **2022**, 13, 5267.
- [6] Z.-G. Zhang, Y. Li, *Angew. Chem., Int. Ed.* **2021**, 60, 4422.
- [7] T. Zhang, Y. Xu, H. Yao, J. Zhang, P. Bi, Z. Chen, J. Wang, Y. Cui, L. Ma, K. Xian, Z. Li, X.-T. Hao, Z. Wei, J. Hou, *Energy Environ. Sci.* **2023**, 16, 1581.
- [8] Y. Li, J. Song, Y. Dong, H. Jin, J. Xin, S. Wang, Y. Cai, L. Jiang, W. Ma, Z. Tang, Y. Sun, *Adv. Mater.* **2022**, 34, 2110155.
- [9] Y. Kong, Y. Li, J. Yuan, L. Ding, *InfoMat* **2022**, 4, e12271.
- [10] M. Zhang, X. Guo, W. Ma, H. Ade, J. Hou, *Adv. Mater.* **2015**, 27, 4655.
- [11] R. Ma, J. Yu, T. Liu, G. Zhang, Y. Xiao, Z. Luo, G. Chai, Y. Chen, Q. Fan, W. Su, G. Li, E. Wang, X. Lu, F. Gao, B. Tang, H. Yan, *Aggregate* **2022**, 3, e58.
- [12] Z. Luo, R. Ma, J. Yu, H. Liu, T. Liu, F. Ni, J. Hu, Y. Zou, A. Zeng, C.-J. Su, U.-S. Jeng, X. Lu, F. Gao, C. Yang, H. Yan, K. Gakuin, *Univ. Nat. Sci. Rev.* **2022**, 9, nwac076.
- [13] C. Sun, F. Pan, H. Bin, J. Zhang, L. Xue, B. Qiu, Z. Wei, Z.-G. Zhang, Y. Li, *Nat. Commun.* **2018**, 9, 743.
- [14] T. Zhang, C. An, Y. Cui, J. Zhang, P. Bi, C. Yang, S. Zhang, J. Hou, *Adv. Mater.* **2022**, 34, 2105803.
- [15] Q. Fan, R. Ma, Z. Bi, X. Liao, B. Wu, S. Zhang, W. Su, J. Fang, C. Zhao, C. Yan, K. Chen, Y. Li, C. Gao, G. Li, W. Ma, *Adv. Funct. Mater.* **2023**, 33, 2211385.
- [16] S. Zhang, Y. Qin, J. Zhu, J. Hou, *Adv. Mater.* **2018**, 30, 1800868.
- [17] Q. Liu, Y. Jiang, K. Jin, J. Qin, J. Xu, W. Li, J. Xiong, J. Liu, Z. Xiao, K. Sun, S. Yang, X. Zhang, L. Ding, *Sci. Bull.* **2020**, 65, 272.
- [18] Y. Xu, Y. Cui, H. Yao, T. Zhang, J. Zhang, L. Ma, J. Wang, Z. Wei, J. Hou, *Adv. Mater.* **2021**, 33, 2101090.
- [19] H. Fu, J. Yao, M. Zhang, L. Xue, Q. Zhou, S. Li, M. Lei, L. Meng, Z.-G. Zhang, Y. Li, *Nat. Commun.* **2022**, 13, 3687.
- [20] L. Ma, S. Zhang, J. Ren, G. Wang, J. Li, Z. Chen, H. Yao, J. Hou, *Angew. Chem., Int. Ed.* **2023**, 62, e202214088.
- [21] C. Yang, S. Zhang, J. Hou, *Aggregate* **2022**, 3, e111.
- [22] D. Jeong, G.-U. Kim, D. Lee, S. Seo, S. Lee, D. Han, H. Park, B. Ma, S. Cho, B. J. Kim, *Adv. Energy Mater.* **2022**, 12, 2201603.
- [23] X. Yuan, Y. Zhao, D. Xie, L. Pan, X. Liu, C. Duan, F. Huang, Y. Cao, *Joule* **2022**, 6, 647.
- [24] X. Yuan, Y. Zhao, Y. Zhang, D. Xie, W. Deng, J. Li, H. Wu, C. Duan, F. Huang, Y. Cao, *Adv. Funct. Mater.* **2022**, 32, 2201142.
- [25] C. Yang, S. Zhang, J. Ren, M. Gao, P. Bi, L. Ye, J. Hou, *Energy Environ. Sci.* **2020**, 13, 2864.
- [26] J. Ren, P. Bi, J. Zhang, J. Liu, J. Wang, Y. Xu, Z. Wei, S. Zhang, J. Hou, *Nat. Sci. Rev.* **2021**, 8, nwab031.
- [27] K. Xian, Y. Geng, L. Ye, *Joule* **2022**, 6, 941.

- [28] Z. Liang, J. He, B. Zhao, M. Gao, Y. Chen, L. Ye, M. Li, Y. Geng, *Sci. China Chem.* **2022**, 66, 216.
- [29] Y. Fu, B. Wang, J. Qu, Y. Wu, W. Ma, Y. Geng, Y. Han, Z. Xie, *Adv. Funct. Mater.* **2016**, 26, 5922.
- [30] Y. Li, Y. Zhang, B. Wu, S. Pang, X. Yuan, C. Duan, F. Huang, Y. Cao, *Sol. RRL* **2022**, 6, 2200073.
- [31] Q. Yang, J. Wang, X. Zhang, J. Zhang, Y. Fu, Z. Xie, *Sci. China Chem.* **2014**, 58, 309.
- [32] K. Zhou, Y. Wu, Y. Liu, X. Zhou, L. Zhang, W. Ma, *ACS Energy Lett.* **2019**, 4, 1057.
- [33] E. Zhou, J. Cong, Q. Wei, K. Tajima, C. Yang, K. Hashimoto, *Angew. Chem., Int. Ed.* **2011**, 50, 2799.
- [34] C. R. McNeill, J. J. M. Halls, R. Wilson, G. L. Whiting, S. Berkebile, M. G. Ramsey, R. H. Friend, N. C. Greenham, *Adv. Funct. Mater.* **2008**, 18, 2309.
- [35] Y. Li, Y. Zhang, B. Wu, S. Pang, X. Yuan, C. Duan, F. Huang, Y. Cao, *Sol. RRL* **2022**, 6, 2200073.
- [36] M. Gao, W. Wang, J. Hou, L. Ye, *Aggregate* **2021**, 2, e46.
- [37] Z. Liang, M. Li, Q. Wang, Y. Qin, S. J. Stuard, Z. Peng, Y. Deng, H. Ade, L. Ye, Y. Geng, *Joule* **2020**, 4, 1278.
- [38] Q. Wang, Y. Qin, M. Li, L. Ye, Y. Geng, *Adv. Energy Mater.* **2020**, 10, 2002572.
- [39] T. Earmme, Y.-J. Hwang, S. Subramaniam, S. A. Jenekhe, *Adv. Mater.* **2014**, 26, 6080.
- [40] T. Earmme, Y.-J. Hwang, N. M. Murari, S. Subramaniam, S. A. Jenekhe, *J. Am. Chem. Soc.* **2013**, 135, 14960.
- [41] X. Jia, Z. Chen, C. Duan, Z. Wang, Q. Yin, F. Huang, Y. Cao, *J. Mater. Chem. C* **2019**, 7, 314.
- [42] J. Xiao, X. Jia, C. Duan, F. Huang, H.-L. Yip, Y. Cao, *Adv. Mater.* **2021**, 33, 2008158.
- [43] X. Yuan, Y. Zhao, T. Zhan, J. Oh, J. Zhou, J. Li, X. Wang, Z. Wang, S. Pang, P. Cai, C. Yang, Z. He, Z. Xie, C. Duan, F. Huang, Y. Cao, *Energy Environ. Sci.* **2021**, 14, 5530.
- [44] R. Sun, W. Wang, H. Yu, Z. Chen, X. Xia, H. Shen, J. Guo, M. Shi, Y. Zheng, Y. Wu, W. Yang, T. Wang, Q. Wu, Y. Yang, X. Lu, J. Xia, C. J. Brabec, H. Yan, Y. Li, J. Min, *Joule* **2021**, 5, 1548.
- [45] Y. Liu, K. Xian, R. Gui, K. Zhou, J. Liu, M. Gao, W. Zhao, X. Jiao, Y. Deng, H. Yin, Y. Geng, L. Ye, *Macromolecules* **2022**, 55, 133.
- [46] N. An, Y. Cai, H. Wu, A. Tang, K. Zhang, X. Hao, Z. Ma, Q. Guo, H. S. Ryu, H. Y. Woo, Y. Sun, E. Zhou, *Adv. Mater.* **2020**, 32, 2002122.
- [47] H. Yao, Y. Cui, D. Qian, C. S. Ponseca Jr., A. Honarfar, Y. Xu, J. Xin, Z. Chen, L. Hong, B. Gao, R. Yu, Y. Zu, W. Ma, P. Chabera, T. Pullerits, A. Yartsev, F. Gao, J. Hou, *J. Am. Chem. Soc.* **2019**, 141, 7743.
- [48] H. Sun, Y. Tang, C. W. Koh, S. Ling, R. Wang, K. Yang, J. Yu, Y. Shi, Y. Wang, H. Y. Woo, X. Guo, *Adv. Mater.* **2019**, 31, 1807220.
- [49] H. Sun, T. Liu, J. Yu, T.-K. Lau, G. Zhang, Y. Zhang, M. Su, Y. Tang, R. Ma, B. Liu, J. Liang, K. Feng, X. Lu, X. Guo, F. Gao, H. Yan, *Energy Environ. Sci.* **2019**, 12, 3328.
- [50] H. Sun, B. Liu, Y. Ma, J.-W. Lee, J. Yang, J. Wang, Y. Li, B. Li, K. Feng, Y. Shi, B. Zhang, D. Han, H. Meng, L. Niu, B. J. Kim, Q. Zheng, X. Guo, *Adv. Mater.* **2021**, 33, 2102635.
- [51] B. Liu, H. Sun, J.-W. Lee, J. Yang, J. Wang, Y. Li, B. Li, M. Xu, Q. Liao, W. Zhang, D. Han, L. Niu, H. Meng, B. J. Kim, X. Guo, *Energy Environ. Sci.* **2021**, 14, 4499.
- [52] D. Shi, Z. Liu, J. Ma, Z. Zhao, L. Tan, G. Lin, J. Tian, X. Zhang, G. Zhang, D. Zhang, *Adv. Funct. Mater.* **2020**, 30, 1910235.
- [53] D. Liu, L. Yang, Y. Wu, X. Wang, Y. Zeng, G. Han, H. Yao, S. Li, S. Zhang, Y. Zhang, Y. Yi, C. He, W. Ma, J. Hou, *Chem. Mater.* **2018**, 30, 619.
- [54] B. Yin, Z. Chen, S. Pang, X. Yuan, Z. Liu, C. Duan, F. Huang, Y. Cao, *Adv. Energy Mater.* **2022**, 12, 2104050.
- [55] B. Xie, K. Zhang, Z. Hu, H. Fang, B. Lin, Q. Yin, B. He, S. Dong, L. Ying, W. Ma, F. Huang, H. Yan, Y. Cao, *Sol. RRL* **2020**, 4, 1900385.
- [56] S. Li, W. Zhao, J. Zhang, X. Liu, Z. Zheng, C. He, B. Xu, Z. Wei, J. Hou, *Chem. Mater.* **2020**, 32, 1993.
- [57] P. Bi, J. Ren, S. Zhang, J. Wang, Z. Chen, M. Gao, Y. Cui, T. Zhang, J. Qin, Z. Zheng, L. Ye, X. Hao, J. Hou, *Nano Energy* **2022**, 100, 107463.
- [58] J. Zhang, Q. Huang, K. Zhang, T. Jia, J. Jing, Y. Chen, Y. Li, Y. Chen, X. Lu, H. Wu, F. Huang, Y. Cao, *Energy Environ. Sci.* **2022**, 15, 4561.
- [59] Z. Wu, C. Sun, S. Dong, X.-F. Jiang, S. Wu, H. Wu, H.-L. Yip, F. Huang, Y. Cao, *J. Am. Chem. Soc.* **2016**, 138, 2004.
- [60] B. Liu, H. Sun, J.-W. Lee, Z. Jiang, J. Qiao, J. Wang, J. Yang, K. Feng, Q. Liao, M. An, B. Li, D. Han, B. Xu, H. Lian, L. Niu, B. J. Kim, X. Guo, *Nat. Commun.* **2023**, 14, 967.
- [61] B. Li, X. Zhang, Z. Wu, J. Yang, B. Liu, Q. Liao, J. Wang, K. Feng, R. Chen, H. Y. Woo, F. Ye, L. Niu, X. Guo, H. Sun, *Sci. China Chem.* **2022**, 65, 1157.
- [62] S. Li, L. Zhan, C. Sun, H. Zhu, G. Zhou, W. Yang, M. Shi, C.-Z. Li, J. Hou, Y. Li, H. Chen, *J. Am. Chem. Soc.* **2019**, 141, 3073.
- [63] C. Li, X. Zhang, N. Yu, X. Gu, L. Qin, Y. Wei, X. Liu, J. Zhang, Z. Wei, Z. Tang, Q. Shi, H. Huang, *Adv. Funct. Mater.* **2022**, 32, 2108861.
- [64] Y. Cai, C. Xie, Q. Li, C. Liu, J. Gao, M. H. Jee, J. Qiao, Y. Li, J. Song, X. Hao, H. Y. Woo, Z. Tang, Y. Zhou, C. Zhang, H. Huang, Y. Sun, *Adv. Mater.* **2023**, 35, 2208165.
- [65] X. Yang, R. Sun, Y. Wang, M. Chen, X. Xia, X. Lu, G. Lu, J. Min, *Adv. Mater.* **2023**, 35, 2209350.
- [66] L. Wang, Q. An, L. Yan, H.-R. Bai, M. Jiang, A. Mahmood, C. Yang, H. Zhi, J.-L. Wang, *Energy Environ. Sci.* **2022**, 15, 320.
- [67] C. Li, J. Zhou, J. Song, J. Xu, H. Zhang, X. Zhang, J. Guo, L. Zhu, D. Wei, G. Han, J. Min, Y. Zhang, Z. Xie, Y. Yi, H. Yan, F. Gao, F. Liu, Y. Sun, *Nat. Energy* **2021**, 6, 605.
- [68] S. Li, Q. Fu, L. Meng, X. Wan, L. Ding, G. Lu, G. Lu, Z. Yao, C. Li, Y. Chen, *Angew. Chem., Int. Ed.* **2022**, 61, e202207397.
- [69] H. Yu, Y. Wang, H. K. Kim, X. Wu, Y. Li, Z. Yao, M. Pan, X. Zou, J. Zhang, S. Chen, D. Zhao, F. Huang, X. Lu, Z. Zhu, H. Yan, *Adv. Mater.* **2022**, 34, 2200361.
- [70] X. Liu, Y. Li, K. Ding, S. Forrest, *Phys. Rev. Appl.* **2019**, 11, 024060.
- [71] N. B. Kolhe, D. K. Tran, H. Lee, D. Kuzuhara, N. Yoshimoto, T. Koganezawa, S. A. Jenekhe, *ACS Energy Lett.* **2019**, 4, 1162.
- [72] Y. Lin, Q. He, F. Zhao, L. Huo, J. Mai, X. Lu, C.-J. Su, T. Li, J. Wang, J. Zhu, Y. Sun, C. Wang, X. Zhan, *J. Am. Chem. Soc.* **2016**, 138, 2973.
- [73] Q. Fan, H. Fu, Q. Wu, Z. Wu, F. Lin, Z. Zhu, J. Min, H. Y. Woo, A. K.-Y. Jen, *Angew. Chem., Int. Ed.* **2021**, 60, 15935.
- [74] Q. Liao, Q. Kang, Y. Yang, C. An, B. Xu, J. Hou, *Adv. Mater.* **2020**, 32, 1906557.
- [75] T. Zhang, Y. Xu, H. Yao, J. Zhang, P. Bi, Z. Chen, J. Wang, Y. Cui, L. Ma, K. Xian, Z. Li, X. Hao, Z. Wei, J. Hou, *Energy Environ. Sci.* **2023**, 16, 1581.
- [76] Z. Zhang, D. Deng, Y. Li, J. Ding, Q. Wu, L. Zhang, G. Zhang, M. J. Iqbal, R. Wang, J. Zhang, X. Qiu, Z. Wei, *Adv. Energy Mater.* **2022**, 12, 2102394.
- [77] J. I. Khan, M. A. Alamoudi, N. Chaturvedi, R. S. Ashraf, M. N. Nabi, A. Markina, W. Liu, T. A. Dela Peña, W. Zhang, O. Alévêque, G. T. Harrison, W. Alsufyani, E. Levillain, S. De Wolf, D. Andrienko, I. McCulloch, F. Laquai, *Adv. Energy Mater.* **2021**, 11, 2100839.
- [78] S.-J. Yoon, K. S. Choi, L. Zhong, S. Jeong, Y. Cho, S. Jung, S. E. Yoon, J. H. Kim, C. Yang, *Small* **2023**, 230057, <https://doi.org/10.1002/sml.202300507>.
- [79] S. Jung, Y. Cho, Y. Ji, J. Oh, G. Park, W. Kim, S. Jeong, S. M. Lee, S. Chen, Y. Zhang, C. Yang, *Nano Energy* **2023**, 106, 108059.
- [80] Y. Li, Q. Li, Y. Cai, H. Jin, J. Zhang, Z. Tang, C. Zhang, Z. Wei, Y. Sun, *Energy Environ. Sci.* **2022**, 15, 3854.
- [81] J. Zhang, C.-H. Tan, K. Zhang, T. Jia, Y. Cui, W. Deng, X. Liao, H. Wu, Q. Xu, F. Huang, Y. Cao, *Adv. Energy Mater.* **2021**, 11, 2102559.
- [82] S. Ma, H. Zhang, K. Feng, X. Guo, *Chem. Eur. J.* **2022**, 28, e202200222.
- [83] M. An, F. Xie, X. Geng, J. Zhang, J. Jiang, Z. Lei, D. He, Z. Xiao, L. Ding, *Adv. Energy Mater.* **2017**, 7, 1602509.

- [84] Y. Liang, D. Zhang, Z. Wu, T. Jia, L. Lüer, H. Tang, L. Hong, J. Zhang, K. Zhang, C. J. Brabec, N. Li, F. Huang, *Nat. Energy* **2022**, 7, 1180.
- [85] Y. Cheng, B. Huang, X. Huang, L. Zhang, S. Kim, Q. Xie, C. Liu, T. Heumüller, Z. Liu, Y. Zhang, F. Wu, C. Yang, C. J. Brabec, Y. Chen, L. Chen, *Angew. Chem., Int. Ed.* **2022**, 61, e202200329.
- [86] B. Liu, Y. Wang, H. Sun, S. Gámez-Valenzuela, Z. Yan, K. Feng, M. A. Uddin, C. Koh, X. Zhou, J. T. L. Navarrete, M. C. R. Delgado, H. Meng, L. Niu, H. Y. Woo, R. Ponce Ortiz, X. Guo, *Adv. Funct. Mater.* **2022**, 32, 2200065.
- [87] H. Chen, S. Y. Jeong, J. Tian, Y. Zhang, D. R. Naphade, M. Alsufyani, W. Zhang, S. Griggs, H. Hu, S. Barlow, H. Y. Woo, S. R. Marder, T. D. Anthopoulos, I. McCulloch, Y. Lin, *Energy Environ. Sci.* **2023**, 16, 1062.
- [88] J. Oh, S. Jung, S.-H. Kang, G. Park, M. Jeong, S. Kim, S. Lee, W. Kim, B. Lee, S. M. Lee, C. Yang, *J. Mater. Chem. A* **2022**, 10, 20606.
- [89] S. Jeong, J. Park, Y. Ji, Y. Cho, B. Lee, M. Jeong, S. Jung, S. Yang, Y. Zhang, S.-J. Yoon, C. Yang, *J. Mater. Chem. A* **2023**, 11, 4703.